

*For publication in A&A*

# Optical and infrared observations of the Crab Pulsar and its nearby knot<sup>\*</sup>

A. Sandberg and J. Sollerman

The Oskar Klein Centre, Department of Astronomy, Stockholm University, AlbaNova, 106 91 Stockholm, Sweden.  
e-mail: jesper@astro.su.se

Preprint online version: October 31, 2018

## ABSTRACT

**Aims.** We study the spectral energy distribution (SED) of the Crab Pulsar and its nearby knot in the optical and in the infrared (IR) regime. We want to investigate how the contribution from the knot affects the pulsar SED in that regime, and examine the evidence for synchrotron self-absorption in the IR. We also draw the attention to the predicted secular decrease in luminosity of the Crab Pulsar, and attempt to investigate this with CCD observations.

**Methods.** We present high-quality  $UBVRIZ$ , as well as adaptive optics  $JHK_sL'$  photometry, achieved under excellent conditions with the FORS1 and NAOS/CONICA instruments at the VLT. We combine these data with re-analyzed archival Spitzer Space Telescope data to construct a SED for the pulsar, and quantify the contamination from the knot. We have also gathered optical imaging data from 1988 to 2008 from several telescopes in order to examine the predicted secular decrease in luminosity.

**Results.** For the Crab Pulsar SED we find a spectral slope of  $\alpha_\nu = 0.27 \pm 0.03$  in the optical/near-IR regime, when we exclude the contribution from the knot. For the knot itself, we find a much redder slope of  $\alpha_\nu = -1.3 \pm 0.1$ . Our best estimate of the average decrease in luminosity for the pulsar is  $2.9 \pm 1.6$  mmag per year.

**Conclusions.** We have demonstrated the importance of the nearby knot in precision measurements of the Crab Pulsar SED, in particular in the near-IR. We have scrutinized the evidence for the traditional view of a synchrotron self-absorption roll-over in the infrared, and find that these claims are unfounded. We also find evidence for a secular decrease in the optical light for the Crab Pulsar, in agreement with current pulsar spin-down models. However, although our measurements of the decrease significantly improve on previous investigations, the detection is still tentative. We finally point to future observations that can improve the situation significantly.

**Key words.** pulsars: individual: The Crab Pulsar

## 1. Introduction

The Crab Nebula and its pulsar are among the most extensively studied objects in astronomical research. The nebula is the remnant of a supernova that was observed in 1054 A.D. Even though well studied, a complete understanding of the supernova that exploded, and the nature of the nebula, is still missing (e.g., Sollerman et al. 2001; Kitaura et al. 2006; Hester 2008; Tziamtzis et al. 2009).

In this paper we focus on the pulsar itself and its immediate environment. The Crab Pulsar has been utilized for decades for testing high-energy astrophysics. But the exact nature of pulsars, including their emission mechanism, is far from fully understood (e.g., Romani 2000). Even in the well studied optical and near-infrared (IR) domain there remain open issues regarding e.g., the origin of the off-pulse polarisation (Shearer & Golden 2002; Słowikowska et al. 2009; Mignani 2009), and the exact spectral-energy-distribution (SED) of the non-thermal emission (Sollerman et al. 2001; O'Connor et al. 2005; Temim et al. 2006) including the influence of the nearby knot, located ap-

proximately  $0''.6$  ( $\sim 1000$  AU) from the pulsar (Hester et al. 1995; Sollerman 2003).

We present new optical and near-IR observations of the Crab Pulsar and its immediate environment in order to trace the SED into the infrared, and to investigate the spectral shape of the emission from the knot. These observations were obtained with the ESO Very Large Telescope (VLT). We also present an attempt to determine the secular decrease of the optical emission by a study of optical CCD imaging data obtained over the past 20 years.

The paper is organized as follows. In Sect. 2 we describe the optical observations obtained under excellent conditions with the FORS1 instrument on the VLT. We also describe the adaptive optics NAOS/CONICA near-IR data from VLT that extend our observations all the way into the  $L'$  band. To extend the SED even further, we also include and re-analyze archival data from the Spitzer Space Telescope. In Sect. 3 we present the SEDs we derive for the pulsar and for the nearby knot, and these results are further discussed in Sect. 4. We also present a complementary investigation of the optical emission from the Crab Pulsar in Sect. 5, where we discuss the evidence for a secular decrease of the  $V$ -band emission from the pulsar using archival data from many telescopes. The paper ends with some conclusions and an outlook in Sect. 6.

<sup>\*</sup> Based on observations made with ESO Telescopes under programme ID 072.D-0029. Tables 3 and 4 and Figure 4 are only available in electronic form via <http://www.edpsciences.org>

## 2. Observations

### 2.1. Optical photometry with FORS1

The Crab Nebula was observed on December 18, 2003, with the FORS1 instrument mounted on UT1 at the VLT. The observations were conducted in service mode to ensure excellent observing conditions. We used the high-resolution mode of the camera, utilizing 0.1 arcsec per pixel. For each of the  $UBVRIZ$  pass-bands, we obtained three dithered exposures. No previous photometry has been reported for the pulsar in the  $z$  band, and this was included in order to tie together the optical and near-IR observations.

The seeing, as measured from the final images, was  $\sim 0''.6$ – $0''.7$  in the  $UBVR$  exposures and  $\sim 0''.7$ – $0''.8$  for the  $I$  and  $z$  bands. For photometric calibrations, the white dwarf spectrophotometric standard star GD 71 (Bohlin et al. 1995) was observed in the  $UBRIz$  bands<sup>1</sup> immediately after the pulsar observations, and at a similar airmass. For the photometric calibration, we have also made use of observations of stars in the Rubin 152 field (Landolt 1992) obtained during the same night.

All FORS1 data were reduced in a standard way, including bias subtraction and flat fielding. We measured the Crab Pulsar and other stars in the field using aperture photometry with an aperture of 8 pixels. The field stars were used for calculating an aperture correction for the pulsar. The background was estimated with an annulus from 25 to 35 pixels in the Crab field, using the centroid sky algorithm.

Point-spread Function (PSF) subtractions were performed on all FORS1 images, using the DAOPHOT algorithm package as implemented in IRAF.<sup>2</sup> This was done in order to remove the pulsar emission and thereby reveal the nearby knot. To reduce the effect of residuals from the pulsar, the knot photometry was performed with an aperture of only 5 pixels, and an aperture correction from 5 to 25 pixels was estimated from the same field stars as for the pulsar. Although the knot is an extended structure, the true width is only  $\sim 0''.2$  (Sect. 4), and the knot can be approximated as a point source for this purpose.

Since no standard  $z$ -band magnitude exists for GD 71, it was estimated by integrating the spectrum of GD 71 under the FORS1 filter profile using the IRAF task `sbands`. For normalization, the same procedure was followed for the spectrum of Vega, and defining its magnitude to zero. When applying this procedure to GD 71, we obtain a  $z$ -band magnitude of  $z = 13.42 \pm 0.03$  for this star. We note that using the same procedure to estimate the  $V$ -band magnitude of GD 71 gives  $V = 13.00$ , which is close to  $V = 13.032 \pm 0.001$  determined by Landolt (1992).

### 2.2. Near-IR adaptive optics with NACO

From October 2003 to September 2004,  $JHK_sL'$  imaging was obtained with the NAOS/CONICA (or NACO, for short) equipment, mounted on the ESO VLT UT4. The  $JHK_s$  observations were performed as an extension of the study previously conducted with the ISAAC instrument (Sollerman 2003, hereafter S03) to study the near-IR properties of the knot. With the NACO adaptive optics system we were able to obtain significantly higher spatial resolution. The pixel scale of these obser-

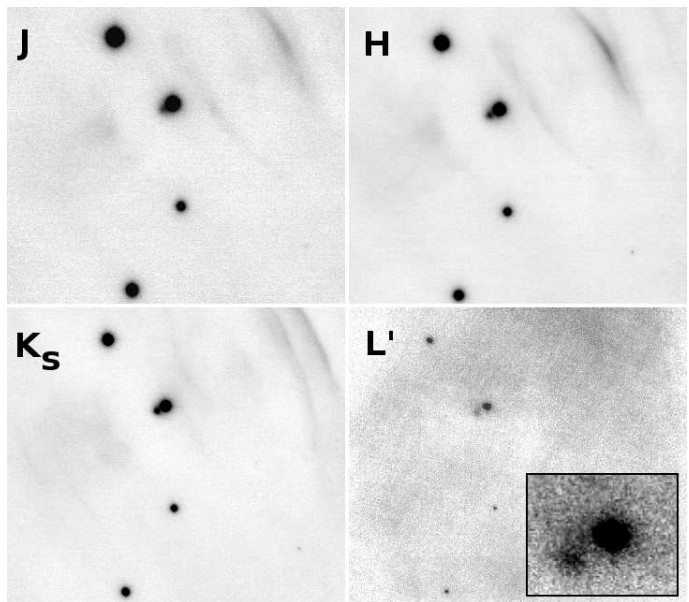


**Fig. 1.** Near-IR NACO images of the Crab Pulsar and its environment. North is up and east is to the left. The field of view is  $\sim 20 \times 18$  arcsec. The pulsar is the lower right of the two bright upper stars. The inlay in the lower right corner shows a close-up of the pulsar and the knot in the  $L'$  band. The field of view for the inset is  $\sim 2.2 \times 1.8$  arcseconds, and the knot positioned 0.6 arcsec south east of the pulsar is easily resolved.

vations were 0.027 arcsec per pixel, and the typical stellar profile in these images have a FWHM of  $\sim 0''.12$  in  $HK_sL'$  and  $\sim 0''.25$  in the  $J$  band. Table 1 is a log of the NACO observations. The  $J$ -band observations, for example, were obtained in sequences of  $3 \times 10$  second exposures to make up the total exposure time shown in the Table, while the  $L'$ -band exposures were conducted using a number of shorter sequences ( $180 \times 0.175$  seconds).

The reductions were performed using the flat and jitter algorithms from the Eclipse software package (see Devillard 1997, for a description of Eclipse). We display our near-IR NACO images in Fig. 1.

The excellent spatial resolution enable us to reveal the contribution from the knot at these wavelengths. To our knowledge, this is the first ground based  $L$ -band image presented of the Crab Pulsar. Our combined  $L'$ -band image consists of almost 3 hours of useful on-source integration time, and highlights the importance of the contribution from the nearby knot at these longer wavelengths (see the lower right inset of Fig. 1).

Albeit adaptive optics is excellent in obtaining improved spatial resolution, it can be difficult to obtain proper absolute flux calibration. We have therefore calibrated our NACO observations using the known magnitudes of four stars in the Crab Pulsar field (from S03, their Table 1). Comparing with the absolute flux calibrated NACO images (using standard stars from Persson et al. 1998), this resulted in corrections to the pulsar magnitudes of order 0.06 mag in the  $JHK$  bands. For the  $L'$  band, we had to rely on the NACO calibration, as obtained from several near-IR standard stars (Leggett et al. 2003). This magnitude estimate thus comes with an additional uncertainty of order  $\sim 0.06$  mags, which is included in Table 2 and Fig. 2.

<sup>1</sup> The  $V$ -band exposure of GD 71 was unfortunately saturated.

<sup>2</sup> IRAF is distributed by the National Optical Astronomy Observatory, which is operated by the Association of Universities for Research in Astronomy (AURA) under cooperative agreement with the National Science Foundation.

Date	Bandpass	Exp. Time (s)
2003-10-18	$K_s$	1260
2004-01-30	$L'$	1228.5
2004-01-31	$H$	1440
2004-01-31	$L'$	1512
2004-02-12	$J$	990
2004-02-12	$L'$	1197
2004-02-13	$L'$	1512
2004-02-22	$L'$	1512
2004-03-13	$L'$	1512
2004-09-15	$L'$	1512

**Table 1.** Log of the NAOS/CONICA  $JHK_sL'$  observations.

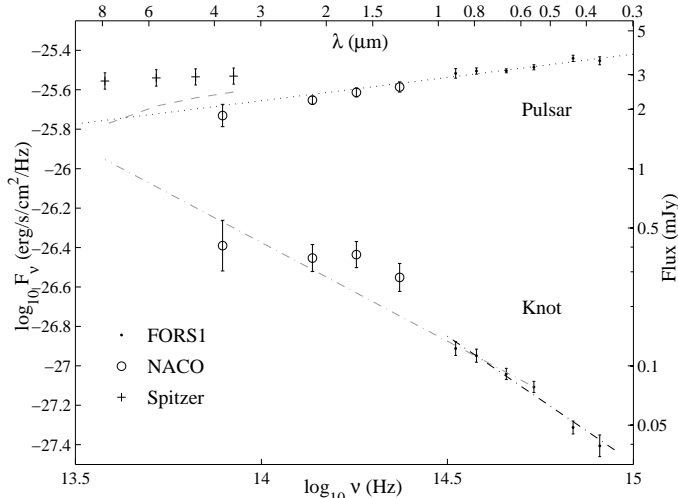


**Fig. 2.** The measured flux of the Crab Pulsar and its knot. The dotted line shows the least-squares fit to the FORS1 and NACO pulsar data, with  $\alpha_\nu = 0.27$ . The black dash-dotted line shows the fitted line to the optical knot flux, with  $\alpha_\nu = -1.3$ . The grey dash-dotted line illustrates a hypothetical extrapolation of the knot flux with a spectral index of  $\alpha_\nu = -1.0$  into the Spitzer wavelength range, and the grey dashed line shows the resultant knot subtracted Spitzer pulsar flux for this assumption.

### 2.3. The Spitzer Space Telescope data

In order to examine the Crab Pulsar further into the mid-infrared, we have also re-analyzed archival data<sup>3</sup> from the Spitzer Space Telescope. These were acquired with the IRAC instrumentation on March 6, 2004. The IRAC observations were made using 12 second exposures and the high dynamic range mode at four dither positions, and the data were previously analysed and published by Temim et al. (2006, hereafter T06).

Spitzer operates in four channels simultaneously, with central wavelengths at approximately 3.6, 4.5, 5.8 and 8.0  $\mu\text{m}$ . For each of the five post-BCD mosaics in each channel, we used an aperture radius of 2 pixels ( $2''.4$ ), with sky annulus radii of 2 to 6 pixels. We then applied the appropriate aperture corrections listed in the IRAC Data Handbook.

## 3. Results

We present our optical  $UBVRIz$ , near-IR  $JHK_sL'$  and the Spitzer Space Telescope magnitudes of the Crab Pulsar and the knot in Table 2. Values for the combination of both pulsar and knot are

**Table 2.** The  $UBVRIz$ ,  $JHK_sL'$  and Spitzer IRAC magnitudes of the Crab Pulsar and its knot.

Bandpass	Crab Pulsar + Knot	Crab Pulsar	Knot
$U$	16.68 $\pm$ 0.03	16.69 $\pm$ 0.03	21.57 $\pm$ 0.13
$B$	17.22 $\pm$ 0.02	17.23 $\pm$ 0.02	21.91 $\pm$ 0.08
$V$	16.64 $\pm$ 0.02	16.66 $\pm$ 0.03	20.72 $\pm$ 0.07
$R$	16.14 $\pm$ 0.01	16.17 $\pm$ 0.02	20.02 $\pm$ 0.07
$I$	15.61 $\pm$ 0.01	15.65 $\pm$ 0.02	19.26 $\pm$ 0.08
$z$	15.35 $\pm$ 0.04	15.39 $\pm$ 0.05	18.88 $\pm$ 0.08
$J$	14.72 $\pm$ 0.03	14.83 $\pm$ 0.03	17.24 $\pm$ 0.06
$H$	14.13 $\pm$ 0.02	14.28 $\pm$ 0.02	16.33 $\pm$ 0.04
$K_s$	13.64 $\pm$ 0.02	13.80 $\pm$ 0.01	15.80 $\pm$ 0.03
$L'$	12.65 $\pm$ 0.08	12.86 $\pm$ 0.07	14.51 $\pm$ 0.15
3.6	12.54 $\pm$ 0.07	...	...
4.5	12.04 $\pm$ 0.07	...	...
5.8	11.55 $\pm$ 0.07	...	...
8.0	10.94 $\pm$ 0.08	...	...

also presented, for comparison to previous studies where the two components could typically not be separated.

Compared to previous measurements, which have been rather inconclusive (see e.g., O'Connor et al. 2005, their Fig. 2), our  $JHK_sL'$  magnitudes agree rather well with the time-resolved measurements of Penny (1982).

For the Spitzer data, we found considerable differences compared to T06. This was found to be due to improper aperture corrections in T06, and updating their measurements, Temim et al. (2009) now obtain results consistent with ours. This changes the slope of the mid-IR measurements significantly.

The spectral energy distribution from the measured flux for the Crab Pulsar, including the NACO and Spitzer data, is shown in Fig. 2. Here we have corrected the flux for interstellar extinction, using the values  $E(B - V) = 0.52$  mag and  $R_V = 3.1$  (Sollerman et al. 2000, hereafter S00). The simplest way to characterize the SED is by a power-law,  $F_\nu = K \nu^{\alpha_\nu}$ , where  $K$  is a constant and the spectral index is denoted  $\alpha_\nu$ . If we fit a linear slope to the FORS1 and NACO data in Fig. 2 we get for the knot subtracted pulsar a spectral index of  $\alpha_\nu = 0.27 \pm 0.03$ .

To estimate the spectral index of the knot we only use the optical FORS1 data. This is because the knot is known to vary in strength, and the NACO data are not contemporaneous. The optical spectral index for the knot obtained in this way is  $\alpha_\nu = -1.3 \pm 0.1$ .

## 4. Discussion of SED data

The measured spectral index of  $\alpha_\nu = 0.27$  for the Crab Pulsar in the optical–near-IR wavelength regime agrees reasonably well with previous studies (see e.g. a compilation of results in Fordham et al. 2002, their Table 6). The exact value of the spectral index depends somewhat on the included wavelength interval, and is slightly flatter for the bluer parts of the ultraviolet to near-IR regime (S00, S03). The value also depends on the applied extinction correction (S00). The novel thing with these measurements is our attempt to remove the contribution from the knot. This will be discussed further below.

The high-resolution NACO data also provide a close view of the pulsar and the knot in the near-IR (Fig. 1). These data can be used in several ways.

The spatial extent of the knot can be estimated from our images. The observed size of  $\sim 0''.25 - 0''.30$  corresponds to a unconvolved extension of  $\sim 0''.22 - 0''.27$ , which is slightly larger than the estimate by Hester et al. (1995) in the optical regime. The

<sup>3</sup> P.I. Robert D. Gehrz.

center of the knot is located at position angle (PA)  $\sim 120^\circ$  from the pulsar, which agrees well with the knot being aligned with the rotation axis of the pulsar (PA  $124^\circ \pm 0.1^\circ$ , Ng & Romani 2004). The knot appears slightly elongated along an axis perpendicular to this, with PA  $\sim 33^\circ$ . As pointed out by Melatos et al. (2005) it is difficult to measure the exact shape of the knot in adaptive optics images where the PSF varies across the field. We do note, however, that the shape of the knot in our NACO images is very similar to that presented by them (Melatos et al. 2005, their Fig. 7).

Our deep  $H$ -band image was used to establish that any counter-knot has to be fainter than  $\sim 2.5\%$  of the knot luminosity. This is somewhat fainter than the limit estimated by Hester et al. (1995) from HST images, who used the absence of a counter-knot to argue for an actual asymmetry in the polar outflow from the pulsar, rather than simply a Doppler boosting effect. However, Doppler boosting has more recently been invoked again to model the knot in MHD simulations (Del Zanna et al. 2006).

Our measurements of the knot also indicate that it is about twice as bright compared to the pulsar in the near-IR compared to the ISAAC measurements of S03. A large variability of this structure (S03, Melatos et al. 2005), as well as other nearby structures (Hester et al. 2002) have also been previously reported.

This variability makes it more difficult to measure the SED of the knot itself. The  $JHK_sL'$  measurements presented in Table 2 were obtained at several different epochs, which is why we have only connected the contemporaneous optical measurements for the knot in Fig. 2. The SED we measure from the optical data is  $\alpha_v = -1.3 \pm 0.1$ . This is a bit redder than the earlier measurement of  $\alpha_v = -0.8$  by S03.

We note, however, that while the measurements by S03 made use of HST images, our FORS images - even though they have the highest quality achievable from the ground - require PSF subtractions that may introduce uncertainties in the measurements. The formal fit error of 0.1 mag may thus underestimate the uncertainties. Having said this, we still speculate if the suggested difference in spectral slope for the knot between these two measurements may be related to the variability of the knot brightness. A multi-band monitoring campaign with the updated HST would be able to investigate such an energy injection emission mechanism for the knot (see Sect. 6.3 for a discussion on future observations).

The observations of S03 did show that the emission of the knot rises strongly into the infrared, and that was part of the motivation for this renewed study. While the knot contributes only  $\sim 1\%$  in the  $U$  band, this knot/pulsar ratio increases to  $\sim 4\%$  in the  $z$  band. The NACO study clearly shows that the knot is even more important in the  $L'$ -band regime, where the knot-to-pulsar ratio amounts to  $22 \pm 8\%$  at this epoch.

Our measurements on the Spitzer data show that the pulsar emission continues with a flat energy distribution all the way out to the longest wavelengths spanned (Fig. 2). The spatial resolution of these data do not allow us to separate the contribution of the pulsar and the knot. The strong contribution of the knot in the  $L'$  band suggests that the knot emission could continue well into the 3-8  $\mu\text{m}$  Spitzer range. This could explain part of the apparent offset for the Spitzer data in Fig. 2. We discuss this further below.

The approximate agreement of the measured spectral index of the pulsar in the optical - near-IR with  $\alpha_v \sim 1/3$  expected for optically thin synchrotron radiation, is a valuable clue for understanding the emission mechanism of pulsars. However, for the

longest wavelengths of measured non-thermal incoherent emission, much of the discussion has traditionally focused on the indication of a possible self-absorption roll-over in the infrared (see references in O'Connor et al. 2005). Our new time-averaged pulsar measurements do not indicate a simple synchrotron self-absorption cut-off (see further discussion in Sect. 6.1).

## 5. The Secular Decrease in Luminosity

Having investigated the SED, we now turn to the possible time evolution of the optical luminosity.

A decrease in the pulsar luminosity by  $\sim 5$  milli-magnitudes (mmag) per year was predicted by Pacini (1971). This secular decrease in luminosity has since been repeatedly claimed, invoked or discussed in the literature (e.g., Kristian 1978; Penny 1982; Pacini & Salvati 1983; Middleditch et al. 1987; Shearer & Golden 2002; Shearer 2008).

The most recent measurement of this decrease in luminosity is from Nasuti et al. (1996). They estimated a decrease of  $8 \pm 4$  mmag  $\text{yr}^{-1}$  in the  $V$  band, but also caution that more observations are needed.

Here we present measurements based on data from the Jacobus Kapteyn Telescope (JKT), the Nordic Optical Telescope (NOT) and the VLT. We concentrate on images obtained in the  $V$ -band over the past 20 years. In this way we are able to increase the number of observations as compared to Nasuti et al. (1996) by a factor of 4, and decrease the individual error bars by a factor of 5. More importantly, this investigation attempts to minimize the systematic uncertainties. Where Nasuti et al. (1996) used a mix of photo-electric time resolved photometry, CCD imaging and photometry derived from a spectrum, we evoke only modern CCD imaging at decent seeing and perform relative photometry against several field stars.

### 5.1. Predicted secular decrease

The predicted decrease in luminosity is based on the simple assumption that the luminosity ( $L$ ) of the pulsar depends on the pulsar period ( $P$ ) as

$$L \propto P^{-n}$$

Pacini (1971) argues that the exponent in the synchrotron luminosity should be  $n \sim 10$  for the Crab Pulsar, and estimated this effect to a secular decrease of 0.005 mag per year. The slightly updated analysis in Pacini & Salvati (1983) argues that this should be observable in the optical pass-bands if the emission is incoherent synchrotron radiation. Using their Equation 10 for optically thin synchrotron emission ( $\alpha_v \sim 1/3$ ), we estimate, using modern values for the pulsar period and period derivative, a predicted secular decrease of 3.8 mmag per year.

### 5.2. Observations of the $V$ -band luminosity

We have gathered archival data from several telescopes. We have used JKT data for 11 epochs between 1988 and 2000, where some of these data were previously used to investigate the wisp motions in the Crab nebula (Tanvir et al. 1997). We have also used data from the NOT from 1998, 2000 and 2008, the above-mentioned FORS1 data from December 2003 as well as additional FORS1 data from November 2003, and FORS2 data from 2005. All these observations were performed in the  $V$ -band filter. A log of the observations is shown in Table 3. These data

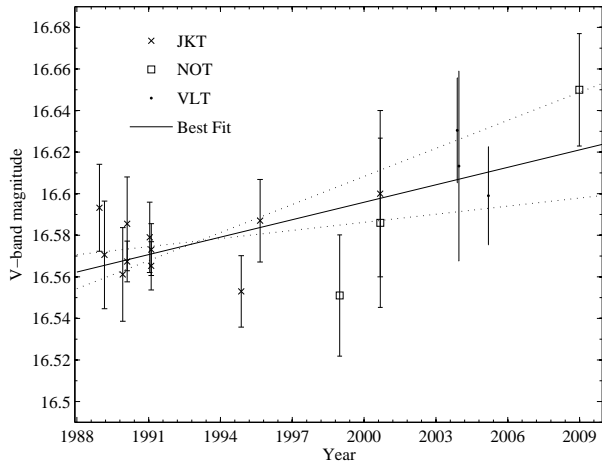


**Fig. 3.** Measured  $V$ -band magnitude of the Crab Pulsar from our investigation of the secular decrease. Crosses mark JKT data, squares NOT data and dots VLT data. The solid line shows the best fit of  $2.9 \text{ mmag/year}$ , with the estimated uncertainties marked by the dotted lines.

include only images with seeing better than  $1.5 \text{ arcsec}$ , in order to minimize errors in background subtraction.

All data were reduced in a standard way. The relative photometry between the Crab Pulsar and 8 stars in the field was performed with PSF photometry, in order to minimize the contribution from the nebula, the wisps and the knot.

To get the zero-point for each exposure we fixed the magnitude of the field star positioned  $6'4 \text{ north}$ ,  $20'6 \text{ east}$  of the pulsar (Star 1 in Table 4 and Fig. 4). Of the 8 well exposed and relatively isolated field stars that we have used, this is the one with  $V$  magnitude most similar to that of the Crab Pulsar, it is close to the pulsar position and was also visible in all images used. The root-mean-square (rms) of the difference in relative photometry for the field stars was then used for estimating the uncertainty in each epoch.

We find that the local standard stars have an rms scatter of  $0.02 \text{ mag}$  over the 17 used epochs. This is thus the precision in photometry we can reach in this study. This is larger than the typical photon noise errors in these frames, and is probably mainly limited by flat fielding errors, but also the neglect of color terms and on the nebular background combined with varying seeing conditions.

### 5.3. Secular Results

The results from our study of the secular decrease in luminosity are shown in Fig. 3. The best (linear least-squares) fit to our data yields an increase of  $2.9 \pm 0.8 \text{ mmag/year}$ . This purely statistical error likely underestimates the uncertainties. We therefore use our 7 independent field stars for comparison, and fit linear slopes also to these. While they rightly show zero evolution on average, the rms scatter on the slopes is  $1.4 \text{ mmag/year}$ . We therefore add this to the uncertainty above, arriving at a final estimate of  $2.9 \pm 1.6 \text{ mmag/year}$ . This is thus a  $2\sigma$  detection of a secular decrease.

## 6. Summary, Discussion and Outlook

We have measured the optical to infrared SED of the Crab Pulsar and its nearby knot. For the pulsar itself, we find a relatively flat spectrum over the entire wavelength range. The spectral index in the optical–near-IR is  $\alpha_v = 0.27 \pm 0.03$ . The nearby knot has a much redder spectrum. We have found that the intensity of the knot can vary by a factor 2. In our  $L'$ -band measurements, the knot contributes almost 20% of the knot+pulsar emission.

In this investigation we have scrutinized two often invoked concepts for the Crab Pulsar, the infrared synchrotron self-absorption (SSA) roll-over, and the secular decrease in luminosity.

### 6.1. Synchrotron Self-absorption

The spectral index of the optical to infrared regime has been discussed in many papers (e.g., S00; S03; Middleditch et al. 1983; Penny 1982; Temim et al. 2006). O'Connor et al. (2005) review the evidence for a SSA roll-over, which is the very basis for their discussion. The notion of an IR SSA is even included in the text books on pulsars (Lyne & Graham-Smith 2005, chapter 19.5). In simple standard theory, such a SSA break would give rise to the longer wavelengths falling off with  $\alpha_v \sim 2 - 2.5$ .

Looking at our time-averaged data, we see in fact no evidence that the slope is steepening away from the  $\alpha_v = 1/3$  expected from simple optically thin synchrotron radiation. In particular, the Spitzer data reveal a flat spectrum all the way out to 8 microns, which does not confirm earlier claims (e.g., Middleditch et al. 1983). Our main conclusion is therefore that there is simply little support for the SSA interpretation in the IR.

We end this section by noting that the nearby knot displays a much redder spectrum, with a spectral index reminiscent of that expected from Fermi-acceleration and cooling behind a shock.

In Fig. 2 we show that if such a  $\alpha_v^{\text{knot}} = -1.0$  extrapolates into the Spitzer region, the knot can indeed contribute substantially in this regime. This could perhaps make the pulsar SED consistent with a  $\alpha_v \sim 1/3$  slope all the way from the UV regime. If the knot is even stronger, the emission detected by Spitzer would in fact mostly be due to the knot, while the pulsar itself must be suppressed by the SSA. Alternatively, the cooling break for the knot occurs before the mid-IR. These speculations can in fact be tested by future observations (Sect. 6.3).

### 6.2. Secular Decrease

We have also investigated the secular decrease of the optical emission of the Crab Pulsar. We note that this effect has been extensively invoked in the literature, but that the observational evidence so far has been meager. In fact, we claim that our investigation is by far the most reliable one to date, but still only indicate a secular decrease at the  $2\sigma$  level. Our measurement agrees well with an updated Pacini's Law, predicting a decrease of  $\sim 4 \text{ mmag/year}$ .

We believe that better estimates of the secular decrease can be obtained (see below). This can not only confirm (or reject) this decrease, but can in detail probe the luminosity evolution of the pulsar and thus the emission mechanism. This is clearly a more direct test on the pulsar evolution than attempts to monitor the synchrotron emission from the entire nebula (e.g., Aller & Reynolds 1985; Reynolds & Chevalier 1984; Smith 2003). For example, in the original  $L = \text{Const.} \times P^{-n}$  formulation of Pacini (1971), our current measurement indicates  $n = 6.8 \pm 3.8$ . While current pulsar emission theory is not yet

very powerful in predicting the exact numbers (e.g., Smith 1981; O'Connor et al. 2005), it is clear that better measurements will be able to discriminate between the  $n = -10$  scenario favoring emission from the proximity of the speed-of-light cylinder, or a significantly shallower index  $n = -4$  if the optical flux scales with the total loss of rotational energy from the neutron star.

### 6.3. Outlook

New observations will be able to resolve several of the above-mentioned issues. Imaging from space (e.g., with the HST) can be used to investigate the optical SED (and any time evolution) of the knot and of the pulsar. In particular, the JWST with sub-arc-second resolution over a large IR wavelength range will be ideal to resolve the knot at the longest wavelengths, and will determine to what extent the knot contributes.

Much of the discrepancies found in published values of the pulsar SED comes from the efforts of patching together broadband magnitudes obtained under varying conditions and with very different instrumentation. The next step to get the pulsar+knot SED would be to use the X-shooter instrument at the VLT to directly probe the spectrum all the way through the optical-NIR.

For the secular decrease it is also evident that more high quality observations will be able to more clearly investigate this effect. Decreasing the errors by a factor 3 would enable interesting comparison to theory, and this is achievable with a uniform dataset. The best possible dataset would of course have been precision measurements with the HST, where a lot of attention has already been directed to studies of the time evolution of the pulsar environment (e.g., Hester et al. 1995; Hester 2008). Unfortunately, the pulsar itself has been categorically saturated in these investigations (see Kaplan et al. 2008), and the existing HST observations are therefore not suitable for investigating the pulsar SED or secular decrease. Other datasets obtained with a uniform telescope/instrument set-up, as e.g., the images used for investigating the expansion of the nebula over time (e.g., Nugent 1998; Trimble 1968; Wyckoff & Murray 1977) could also be of interest. We note that there must exist significantly more data which could be useful for this type of analysis. We therefore encourage the astronomical community to investigate or share their Crab Pulsar images.

*Acknowledgements.* This paper is based on results from the master thesis of Andreas Sandberg. Jesper Sollerman is a Royal Swedish Academy of Sciences Research Fellow supported by a grant from the Knut and Alice Wallenberg Foundation. The Oskar Klein Centre is funded by the Swedish Research Council (VR), and A. Sandberg acknowledge further support from VR. We thank the anonymous referee for a concise report. We thank Tea Temim for a fruitful conversation on the Spitzer data reductions, Yura Shibano for pointing us in that direction and N. & P. Lundqvist for early discussions on this project. Claes-Ingvar Björnsson is thanked for many discussions on the theoretical aspects of this work, and we thank M. Persson for the Albanova Telescope images and W. Nowotny for the NOT images from 2000. Some of the data presented here have been taken using ALFOOSC, which is owned by the Instituto de Astrofísica de Andalucía (IAA) and operated at the Nordic Optical Telescope under agreement between IAA and the NBI in Copenhagen. This paper also makes use of data obtained from the Isaac Newton Group Archive which is maintained as part of the CASU Astronomical Data Centre at the Institute of Astronomy, Cambridge. This work is based in part on observations made with the Spitzer Space Telescope, which is operated by the Jet Propulsion Laboratory, California Institute of Technology under a contract with NASA.

## References

- Aller, H. D., & Reynolds, S. P. 1985, *ApJ*, 293, L73  
 Böhlín, R. C., Colina, L., & Finley, D. S. 1995, *AJ*, 110, 1316  
 Del Zanna, L., Volpi, D., Amato, E., & Bucciantini, N. 2006, *A&A*, 453, 621  
 Devillard, N. 1997, *The Messenger*, 87, 19  
 Fordham, J. L. A., Vranesević, N., Carramiñana, A., Michel, R., Much, R., Wehinger, P., & Wyckoff, S. 2002, *ApJ*, 581, 485  
 Hester, J. J., et al. 2002, *ApJ*, 577, L49  
 Hester, J. J. 2008, *ARA&A*, 46, 127  
 Hester, J. J., et al. 1995, *ApJ*, 448, 240  
 Kaplan, D. L., Chatterjee, S., Gaensler, B. M., & Anderson, J. 2008, *ApJ*, 677, 1201  
 Kitaura, F. S., Janka, H.-T., & Hillebrandt, W. 2006, *A&A*, 450, 345  
 Kristian, J. 1978, *BAAS*, 10, 425  
 Landolt, A. U. 1992, *AJ*, 104, 340  
 Leggett, S. K., et al. 2003, *MNRAS*, 345, 144  
 Lyne, A. G., & Graham-Smith, F. 2005, *Pulsar Astronomy*, by Andrew G. Lyne and Francis Graham-Smith, ISBN 0521839548. Cambridge, UK: Cambridge University Press, 2005.  
 Melatos, A., et al. 2005, *ApJ*, 633, 931  
 Middleditch, J., Pennypacker, C. R., & Burns, M. S. 1987, *ApJ*, 315, 142  
 Middleditch, J., Pennypacker, C. R., & Burns, M. S. 1983, *ApJ*, 273, 261  
 Mignani, R. P. 2009, arXiv:0902.0631  
 Nasuti, F. P., Mignani, R., Caraveo, P. A., & Bignami, G. F. 1996, *A&A*, 314, 849  
 Ng, C.-Y., & Romani, R. W. 2004, *ApJ*, 601, 479  
 Nugent, R. L. 1998, *PASP*, 110, 831  
 O'Connor, P., Golden, A., & Shearer, A. 2005, *ApJ*, 631, 471  
 Pacini, F. 1971, *ApJ*, 163, L17  
 Pacini, F., & Salvati, M. 1983, *ApJ*, 274, 369  
 Penny, A. J. 1982, *MNRAS*, 198, 773  
 Persson, S. E., Murphy, D. C., Krzeminski, W., Roth, M., & Rieke, M. J. 1998, *AJ*, 116, 2475  
 Reynolds, S. P., & Chevalier, R. A. 1984, *ApJ*, 278, 630  
 Romani, R. W. 2000, *Highly Energetic Physical Processes and Mechanisms for Emission from Astrophysical Plasmas*, 195, 95  
 Słowikowska, A., Kanbach, G., Kramer, M., & Stefanescu, A. 2009, arXiv:0901.4559  
 Shearer, A., & Golden, A. 2002, *Neutron Stars, Pulsars, and Supernova Remnants*, 44  
 Shearer, A. 2008, *Astrophysics and Space Science Library*, 351, 1  
 Smith, F. G. 1981, *Pulsars: 13 Years of Research on Neutron Stars*, 95, 221  
 Smith, N. 2003, *MNRAS*, 346, 885  
 Sollerman, J. 2003, *A&A*, 406, 639  
 Sollerman, J., Kozma, C., & Lundqvist, P. 2001, *A&A*, 366, 197  
 Sollerman, J., Lundqvist, P., Lindler, D., Chevalier, R. A., Fransson, C., Gull, T. R., Pun, C. S. J., & Sonneborn, G. 2000, *ApJ*, 537, 861  
 Tanvir, N. R., Thomson, R. C., & Tsikarishvili, E. G. 1997, *New Astronomy*, 1, 311  
 Temim, T., et al. 2006, *AJ*, 132, 1610  
 Temim, T., et al. 2009, *AJ*, 137, 5155  
 Trimble, V. 1968, *AJ*, 73, 535  
 Tziamtzis, A., Schirmer, M., Lundqvist, P., & Sollerman, J. 2009, *A&A*, 497, 167  
 Wyckoff, S., & Murray, C. A. 1977, *MNRAS*, 180, 717

Date	Telescope	Instrument/Detector	Exposure Time (s)	Seeing	Stars Not Included
1988-12-11	JKT	GEC4	$7 \times 1000$	1".4	4,5
1989-02-26	JKT	GEC3	$2 \times 1000$	1".4	5
1989-12-02	JKT	RCA2	$3 \times 1000$	1".3	...
1990-02-07	JKT	GEC3	$2 \times 1000$	1".1	...
1990-02-08	JKT	GEC3	$5 \times 1000$	1".1	...
1991-01-17	JKT	GEC3	$3 \times 1000$	1".2	...
1991-02-09	JKT	GEC3	$4 \times 1000$	1".4	2
1991-02-10	JKT	GEC3	$3 \times 1000$	1".2	2
1994-11-14	JKT	TEK4	$1 \times 1200$	1".3	5(S),6(S),7(S)
1995-08-28	JKT	TEK4	$1 \times 300$	1".4	...
1998-12-25	NOT	LORAL	$1 \times 30$	1".4	...
2000-09-03	JKT	SITe2	$1 \times 250$	1".1	...
2000-09-04	NOT	LORAL	$1 \times 300$	0".9	...
2003-11-23	VLT	FORS1	$2 \times 5$	0".7	...
2003-12-18	VLT	FORS1	$3 \times 20$	0".6	...
2005-03-12	VLT	FORS2	$1 \times 0.987$	1".3	5,9
2008-12-19	NOT	EEV	$3 \times 180$	0".9	...

**Table 3.** V-band data used for examining the secular decrease in luminosity of the Crab Pulsar. The final column lists stars that are saturated (S) or outside the field of view in the particular image, and the numbers refer to Table 4 and Fig. 4.

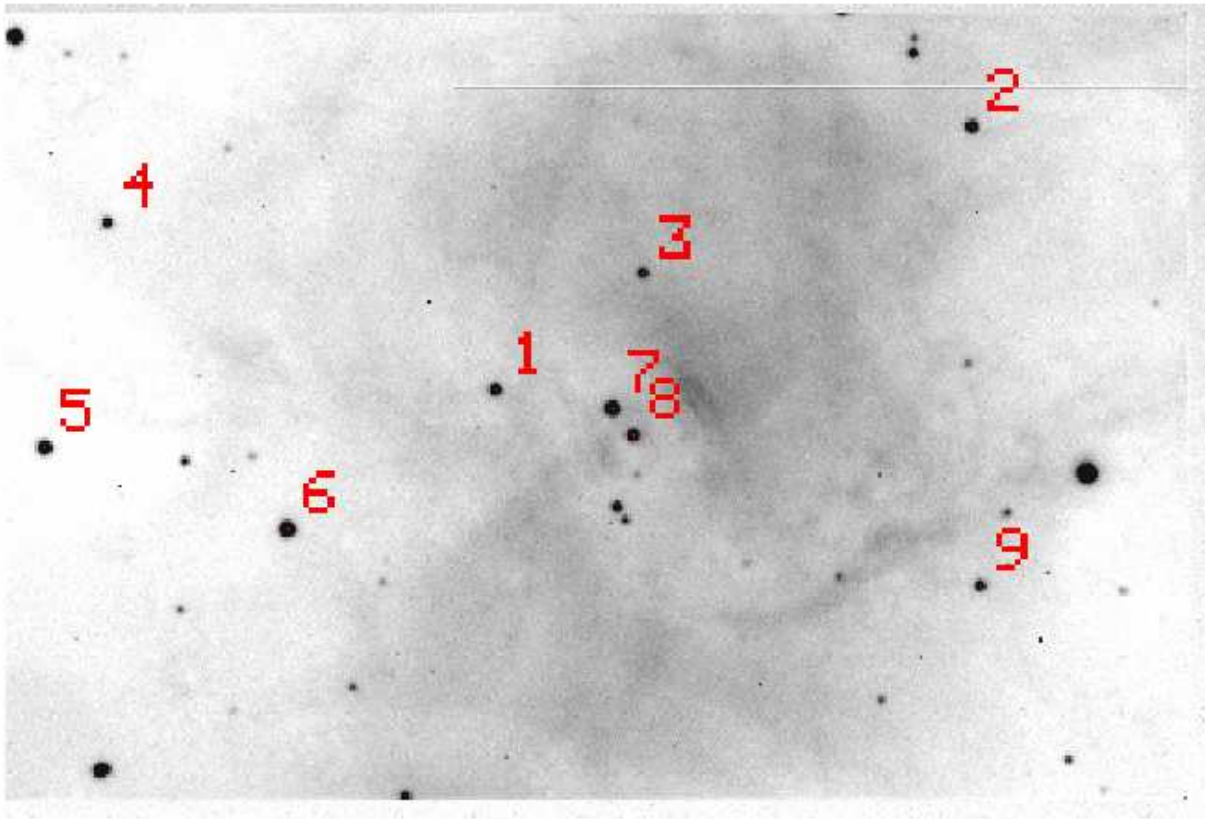


**Fig. 4.** The stars that were chosen for relative photometry in the investigation of the secular decrease in luminosity. The numbering is the same as in Table 4 where the  $UBVRIz$  magnitudes for these stars are given. The numbering is also used in Table 3. The pulsar is number eight. This V-band image was acquired with the JKT on February 7 1990. North is up and east is to the left. The field of view is approximately 3.2 by 2.1 arcminutes.

Star No.	U	B	V	R	I	z
1	17.80	17.49	16.51	15.92	15.36	15.13
2	18.43	17.74	16.36	15.59	14.87	14.53
3	18.42	18.29	17.40	16.82	16.26	16.02
4	18.74	18.32	17.16	16.48	15.86	15.59
5	18.45	17.23	15.64	14.80	14.07	13.71
6	16.56	16.29	15.37	14.78	14.22	13.98
7	16.80	16.64	15.79	15.25	14.74	14.52
9	18.13	17.93	17.07	16.51	15.97	15.75

**Table 4.**  $UBVRIz$  magnitudes of the eight field stars examined in the secular decrease of luminosity of the pulsar. The typical errors in  $VRI$  are 0.02 mags, while  $B$ ,  $z$  and  $U$  give uncertainties of 0.03, 0.04 and 0.05 respectively. These magnitudes were estimated with the FORS1 calibrations described in Section 2.1. The numbering corresponds to Fig. 4 and Table 3.